Modeling of Permanent-Magnet Synchronous Machine Including Torque Ripple Effects

Abraham Gebregergis, *Senior Member, IEEE*, Mazharul Huq Chowdhury, *Senior Member, IEEE*, Mohammad S. Islam, *Senior Member, IEEE*, and Tomy Sebastian, *Fellow, IEEE*

***Abstract*—A model of permanent-magnet synchronous machine (PMSM), including the electromagnetically originated torque ripple, is presented in this paper. This unique representation of such equivalent circuit is highly critical to understand the torque ripple content and to develop an appropriate mitigation scheme for low torque ripple applications requiring four quadrant operations. This research proposes a method to quantify the various sources of torque ripple and modifies the existing dq-model to enhance the modeling capabilities for both surface-mount and interior PMSMs. Finite-element (FE) analysis is used for modeling various PMSMs to verify the lumped circuit model proposed in this research. The theoretical results obtained from analytical and FE analysis are validated using experimental test.**

***Index Terms*—Electric machines, finite-element (FE) methods, modeling, permanent-magnet (PM) motor, torque control.**

I. Introduction

THE high power density and low torque ripple characteristics of the permanent-magnet synchronous machine (PMSM) makes it an ideal candidate for high-performance applications. The interior PM (IPM) synchronous machines are getting more attention for better PM material utilization relative to the surface mount PM (SPM) machines [1]. IPM machines typically use cheaper rectangular magnets inserted inside the rotor core, which improves magnet retention and manufacturing yields [2]. The torque production mechanism in an IPM is a combination of the reaction torque generated by the interaction between the PMs mounted on the rotor and the stator mmf and the reluctance torque produced due to the saliency between direct and quadrature axis in contrast SPM motors that only have the reaction torque. Generally, due to the simple rectangular magnet shape and use of concentrated winding, the torque ripple developed in an IPM is higher. In order to minimize the sources by design or to develop an active cancellation of torque ripple, it is important to understand the behavior and quantify the sources of torque ripple. In this paper, the existing dq-model [3]–[5] will be augmented to provide additional capabilities for predicting the performance of PM motors, including IPM motors using the analytical model. Rojas *et al.* [6] presented an analytical torque computation based on an energy approach, including the torque ripple harmonic components. Reducing of the torque ripple using different methods is discussed in [7]–[12]. These methods lack modeling of the torque ripple components.

This paper focuses on modeling and quantifying the source of torque ripple as part of the dq-model of PMSM. Finite-element (FE) analysis tool is used to study and quantify the sources of torque ripple contents. These sources are identified as due to the interaction of the PM's originated flux density and the rotor saliency with the mmf resulted due to the space distribution of the winding in the stator. The effect of each source is separately identified and modeled as a voltage source added to the existing dq-model of PMSM. Each added element in the enhanced dq-model is derived and validated by extensive FE simulation, which is later validated by experimental tests.

Manuscript received December 18, 2013; revised March 28, 2014; accepted May 28, 2014. Date of publication July 8, 2014; date of current version January 16, 2015. Paper 2013-EMC-0967.R1, presented at the 2013 IEEE Energy Conversion Congress and Exposition, Denver, CO, USA, September 16–20, and approved for publication in the IEEE TRANSACTIONS ON INDUSTRY APPLICATIONS by the Electric Machines Committee of the IEEE Industry Applications Society.

The authors are with Halla Mechatronics, Bay City, MI 48706 USA (e-mail: abraham.Gebregergis@halla.com; sajib_eee2000@yahoo.com; mohammad.s.islam@ieee.org; tomy.sebastian@halla.com).

Color versions of one or more of the figures in this paper are available online at http://ieeexplore.ieee.org.

Digital Object Identifier 10.1109/TIA.2014.2334733

II. Modeling of PMSMs

A. Basic dq-Model of PMSM

The dynamic model of a PMSM in the dq-reference frame is given by (1)–(5) [3]–[5]

$$V_{dq0} = KV_{abc} \tag{1}$$

$$K = \frac{2}{3}\begin{bmatrix} -\cos(\omega_e t) & -\cos(\omega_e t-120) & -\cos(\omega_e t-240) \\ \sin(\omega_e t) & \sin(\omega_e t-120) & \sin(\omega_e t-240) \\ \frac{1}{2} & \frac{1}{2} & \frac{1}{2} \end{bmatrix} \tag{2}$$

$$V_{abc} = Ri_{abc} + e_{abc} + \frac{d(L_{abc}i_{abc})}{dt} \tag{3}$$

$$\begin{bmatrix} V_d \\ V_q \end{bmatrix} = \begin{bmatrix} R & -\omega_e L_q \\ \omega_e L_d & R \end{bmatrix}\begin{bmatrix} i_d \\ i_q \end{bmatrix} + \begin{bmatrix} 0 \\ \omega_m K_{mq0} \end{bmatrix} + \begin{bmatrix} L_d \\ L_q \end{bmatrix}\frac{d}{dt}\begin{bmatrix} i_d \\ i_q \end{bmatrix} \tag{4}$$

$$T_e = \frac{3}{2}K_{qm0}i_q - \frac{3P}{4}i_q i_d(L_q - L_d) \tag{5}$$

$$\omega_e = \frac{P}{2}\omega_m \tag{6}$$

where K is the Park's transformation matrix, V_{abc} is the phase voltage, i_{abc} is the phase current, R is the resistance of the machine, L_q and L_d are the q- and d-axis inductances, respectively. i_q, i_d, V_q, and V_d are the q- and d-axis currents and voltages,

respectively. K_{qm0} is the motor back EMF constant, whereas w_m and w_e are the mechanical and electrical motor speeds, respectively. T_e is the developed electromagnetic torque, and P is the number of poles of the machine.

B. Enhanced dq-Model of PMSM Including Torque Ripple

The dynamic model of a PMSM described in the aforementioned section is modified to include the torque ripple contents. The developed electromagnetic torque and ripple contribution due to the interaction between the flux density produced by the PMs on the rotor and the mmf produced by current-carrying windings distributed in space of the stator can be modeled in two steps, namely, reaction and reluctance parts, respectively. In IPM rotor configuration, both reaction and reluctance portions can be modeled as follows:

i) *Interaction of Airgap Flux Density and Stator MMF*

The torque developed due to the interaction between airgap flux density produced by the PMs and applied current can be expressed as given in

$$T_m = \frac{3}{2}(I_q K_{qm0} + I_q K_{qm} + I_d K_{dm}) \tag{7}$$

where

$$K_{qm} = \sum_{n=6}^{\infty} K_{qmn} \cos(n\theta + \alpha_{qmn}) \tag{8}$$

$$K_{dm} = \sum_{n=6}^{\infty} K_{dmn} \cos(n\theta + \alpha_{dmn}) \tag{9}$$

where $n = 6, 12$, *and 18*; K_{qm0} is the average torque constant; K_{xm6}, K_{xm12}, and K_{xm18} are the amplitudes of 6th-, 12th-, and 18th-order components of motor torque constants; and α_{xw6}, α_{xw12}, and α_{xw18} are the phase shifts of the 6th-, 12th-, and 18th-order harmonics of the motor torque constants; and x denotes q- or d-axis; and m is the magnet contribution. Note that (7)–(9) are adequate to express torque and ripple contents for SPM motors.

ii) *Interaction of Saliency of the Rotor and Stator MMF*

Both q-axis and d-axis currents contribute into the developed torque due to the interaction between the saliency of the rotor and stator mmf, as expressed by (10). The torque ripple components in dq-reference frame can be expressed as

$$T_w = \frac{3}{2}(I_q K_{qw} + I_d K_{dw}) \tag{10}$$

$$K_{qw} = \sum_{n=6}^{\infty} K_{qwn} \cos(n\theta + \alpha_{qwn} + \beta), \quad n = 6, 12, 18, \text{etc.} \tag{11}$$

$$K_{dw} = \sum_{n=6}^{\infty} K_{dwn} \cos(n\theta + \alpha_{dwn} + \beta), \quad n = 6, 12, 18, \text{etc.} \tag{12}$$

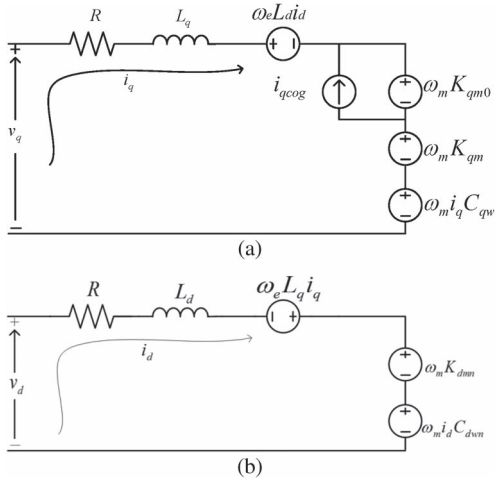

Fig. 1. Enhanced equivalent circuit of PMSM. (a) q-axis circuit. (b) d-axis circuit.

where K_{qw} and K_{dw} are the q- and d-axes time varying motor torque values; K_{qw6}, K_{qw12}, and K_{qw18} are the amplitudes; and α_{qw6}, α_{qw12}, and α_{qw18} are the phase shifts of the 6th-, 12th-, and 18th(nth)-order harmonics of the motor torque constant in the q-axis; whereas K_{dw6}, K_{dw12}, and K_{dw18} are the amplitudes; and α_{dw6}, α_{dw12}, and α_{dw18} are the phase shifts of 6th-, 12th-, and 18th-order harmonics of the motor torque constant in the d-axis due to rotor saliency and stator winding space distribution. β is the phase angle of the applied current with respect to q-axis.

Equation (13) represents the enhanced dq-model of the PMSM, which is also shown in Fig. 1 as the lumped circuit model, where C_{qwn} and C_{dwn} are the motor torque constants due to rotor saliency and stator winding space distribution. The total torque, including the torque ripple due to the airgap flux density produced by PMs, stator winding space distribution, rotor saliency and current, the cogging torque is expressed by (14). The inclusion of the additional terms in (13) and (14) compared with the model expressed in (4) uniquely brings completeness to the existing model in predicting torque ripple mechanism in PMSMs. The model is generally applicable to both SPM and IPM motor configurations

$$\begin{bmatrix} V_d \\ V_q \end{bmatrix} = \begin{bmatrix} R & -\omega_e L_q \\ \omega_e L_d & R \end{bmatrix} \begin{bmatrix} i_d \\ i_q \end{bmatrix} + \begin{bmatrix} 0 \\ \omega_m K_{qm0} \end{bmatrix} + \begin{bmatrix} \omega_m K_{dmn} \\ \omega_m K_{qmn} \end{bmatrix} + \begin{bmatrix} \omega_m K_{dwn} \\ \omega_m K_{qwn} \end{bmatrix} + \begin{bmatrix} L_d \\ L_q \end{bmatrix} \frac{d}{dt} \begin{bmatrix} i_d \\ i_q \end{bmatrix} \tag{13}$$

$$T_e = \frac{3}{2}(K_{qm0} + K_{qmn} + K_{qwn}) i_q + \frac{3}{2} i_{\text{cog}} K_{qm0} + \frac{3}{2}(K_{dmn} + K_{dwn}) i_d - \frac{3}{2}\frac{P}{2} i_q i_d (L_q - L_d). \tag{14}$$

i_{qcog} can be obtained by measuring the cogging torque of the test motor T_{cog} and using (15), where K_{mq0} is the

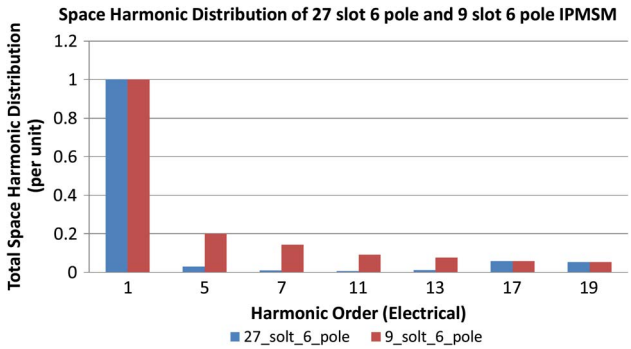

Fig. 2. Space harmonic distribution of 27-slot and 9-slot 6-pole IPMSM.

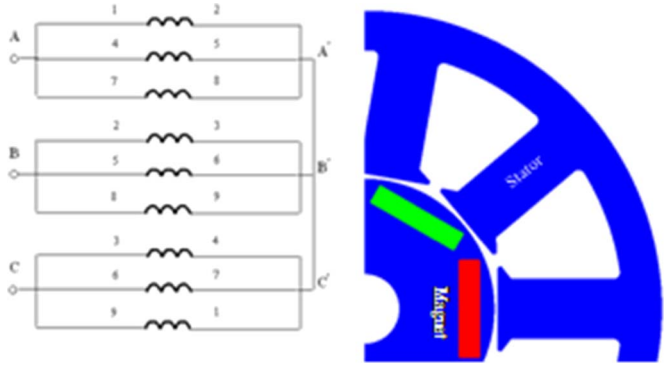

Fig. 3. Winding and circuit configuration to simulate electromagnetic torque simulation.

average back EMF constant

$$i_{qcog} = \frac{2}{3} T_{cog} / K_{qm0}. \tag{15}$$

iii) *Effect of Stator Slot on MMF Distribution*

The space distribution of the winding depends on the number of slots. It is impossible to distribute the winding in sinusoidal fashion using a finite number of slots. The constants K_{qwn} and K_{dwn} are a function of the $n \pm 1$th stator mmf space distribution and the rotor saliency. Fig. 2 shows the space harmonics in the mmf distribution of a 9-slot-6-pole and 27-slot-6-pole PMSM. The magnitude of the space harmonics distribution of the 27-slot 6-pole design is lower than the 9-slot 6-pole. Therefore, the 27-slot-6-pole has less torque ripple produced for the same rotor saliency due to the reduction in the space distribution harmonics, as shown in Fig. 2. A 9-slot 6-pole SPM has lower torque ripple than a 9-slot-6-pole IPM due to the insignificant rotor saliency in SPM. The mmf space distribution of a 27-slot 6-pole and 9-slot 6-pole PMSM can be computed using the (16) for a pure sinusoidal current through the conductors. However, the coefficient b_n is different between the two motor topologies

$$F = \begin{cases} -\frac{3}{2} I_p N \sum_{n=1}^{\infty} b_n \cos(wt + n\theta), & \text{for } n = 3k+1; \\ & k = 0, 1, 2, 3, \ldots \\ \frac{3}{2} I_p N \sum_{n=1}^{\infty} b_n \cos(wt - n\theta), & \text{for } n = 3k-1; \\ & k = 1, 2, 3, \ldots \end{cases} \tag{16}$$

where F is the total mmf, I_p is the peak current, and N is the number of turns.

For a 27-slot 6-pole machine, the value of b_n can be written as

$$b_n = \begin{cases} 0, & \text{for } n \text{ is even} \\ \frac{4}{\pi n} \sin\left(\frac{\pi}{2} n\right)\left[\sin\left(\frac{\pi}{3} n\right) + 2\sin\left(\frac{4\pi}{9} n\right)\right] & \text{otherwise.} \end{cases} \tag{17}$$

Similarly, for a 9-slot 6-pole machine, the value of b_n is

$$b_n = \begin{cases} 0, & \text{for } n \text{ is even} \\ \frac{4}{\pi n} \sin\left(\frac{\pi}{2} n\right) \sin\left(\frac{\pi}{3} n\right) & \text{otherwise.} \end{cases} \tag{18}$$

Equations (17) and (18) are developed assuming point conductors placed at the center of the stator slot opening. In reality, it can be assumed that the conductors are distributed in the stator slot opening. This distribution reduces the harmonics in the mmf distribution. For example, in the case of 27-slot 6-pole machine, the real value of the 17th- and 19th-order harmonics will be lower. Similarly for a 9-slot 6-pole machine, the 5th- and 7th-, and 17th- and 19th-order harmonics will be reduced due to the conductor distribution in the stator slot opening.

III. FE Modeling of PMSM

A 9-slot 6-pole three-phase IPMSM shown in Fig. 3 is used during this research. The winding of each phase has three parallel paths. A 2-D FE model is developed and used for the analysis to calculate the open-circuit voltage and to evaluate the electromagnetic torque when excited with balanced three-phase currents, whereas the motor is running at a constant speed. In order to separate the torque ripple due to the rotor magnet and the rotor saliency, the electromagnetic torque is calculated with the magnet remanence Br set to zero and with the Br set to the actual value. This approach is done to study the effect of magnet and saliency issues separately on the torque ripple and to create an equivalent circuit model.

A. Open-Circuit Test

The open-circuit simulation is done at 1000 r/min mechanical, with the terminals of the motor disconnected from the source. The flux linkage through each phase is captured and is used to calculate the induced voltage. The instantaneous value of the motor back EMF constants Ke_{ph} of each phase is calculated by dividing the induced voltage (v_{ind}) by the motor speed (ω_m) as given in (19). These per phase motor back EMF constants in abc-frame are transformed into dq-axis using Park's transformation. Fig. 4 shows the harmonic contents of the motor back EMF constant in the abc- and dq-reference frame

$$K_{\text{eph}} = \frac{v_{\text{ind}}}{\omega_m}. \tag{19}$$

B. Electromagnetic Torque Simulation Without Magnet $(Br = 0)$

This simulation is performed setting the magnet Br to zero to study the torque ripple effect due to the interaction of winding

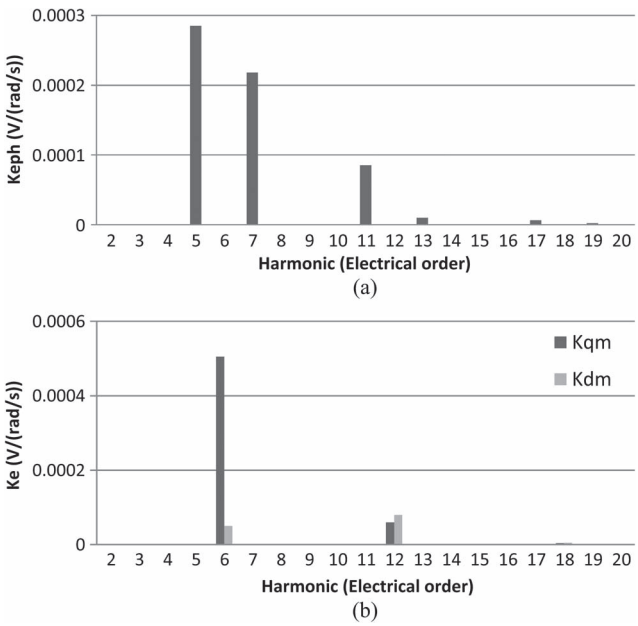

Fig. 4. Back EMF motor constant. (a) *abc*-frame. (b) *dq*-axis.

space distribution with the rotor saliency, whereas the motor is fed by balanced sinusoidal currents. The simulation is done at various current magnitudes and phases. The first set of simulations involves a peak current of 25, 50, 75, 100, 125, and 133 A and zero phase shift with respect to the back EMF. In this particular scenario, we will vary the current in q-axis, whereas the current in d-axis is zero. Developed electromagnetic torque is captured from the FE simulation under these conditions. The peak value of the motor constant K_{qw6} in q-axis is calculated from the torque and applied q-axis current. Fig. 5 shows the peak of sixth-order torque ripple and peak of sixth-order motor constant K_{qw6}. The sixth-order peak value of the motor constant K_{qw6} is linearly proportional to the applied q-axis current. Therefore, the sixth-order peak motor constant K_{qw6} and peak torque ripple T_{qw6} as a function of q-axis current (i_q) can be written as

$$K_{qw6} = c_{q6} i_q \tag{20}$$

$$T_{qw6} = \frac{3}{2} c_{q6} i_q^2. \tag{21}$$

The d-axis current effect can be studied similar to the q-axis current for the following peak currents of 25, 50, 75, 100, 125, and 133 A, whereas the current phase angle is shifted to 90°. In this particular scenario, we will vary the current in d-axis, whereas the current in q-axis is zero. The peak value of the motor constant K_{dw6} is calculated from the developed torque and d-axis current. Fig. 6 shows the sixth-order harmonic peak torque ripple and sixth-order harmonic peak motor constant K_{dw6}. The peak value of motor constant K_{dw6} is linearly proportional to the applied d-axis current i_d. Therefore, the sixth-order peak motor constant K_{dw6} and peak torque ripple T_{dw6} as a function of the d-axis current i_d can be written as

$$K_{dw6} = c_{d6} i_d \tag{22}$$

$$T_{dw6} = \frac{3}{2} c_{d6} i_d^2. \tag{23}$$

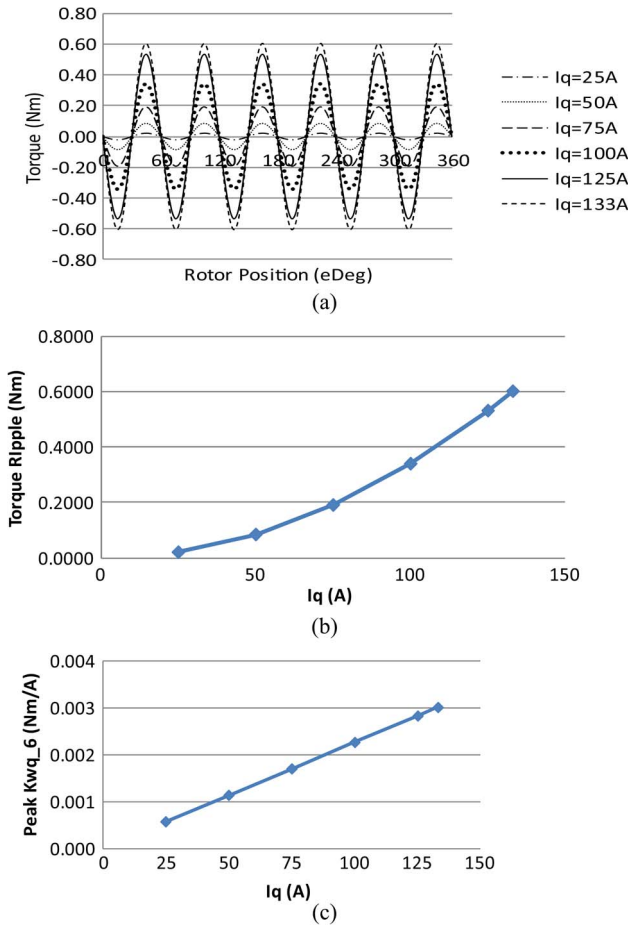

Fig. 5. (a) Developed electromagnetic torque by varying q-axis current and $I_d = 0$ A. (b) Sixth-order torque ripple magnitude. (c) Sixth-order motor constant magnitude.

In both conditions, the average developed electromagnetic torque is zero. A similar approach can be used to derive the relationship between the 12th-order torque ripple and applied current. In general, the nth order (where $n = 6$, 12, 18, etc.) torque ripple and motor torque constants can be expressed as

$$K_{qwn} = c_{qn} i_q \tag{24}$$

$$T_{qwn} = \frac{3}{2} c_{qn} i_q^2 \tag{25}$$

$$K_{dwn} = c_{dn} i_d \tag{26}$$

$$T_{qwn} = \frac{3}{2} c_{dn} i_d^2. \tag{27}$$

In Figs. 5(a) and 6(a), the phase of the torque ripple is shifted by 180° as seen in the plots when the applied current waveform is shifted by 90°. This phase reversal is due to the torque and current relation as defined by a square function. The phase shift is independent of the peak current magnitude.

C. Electromagnetic Torque Simulation With PMs $(Br \neq 0)$

The combined effect of flux density produced by PMs, rotor saliency, and the winding space distribution on the developed torque is studied by placing the PMs on the rotor and running

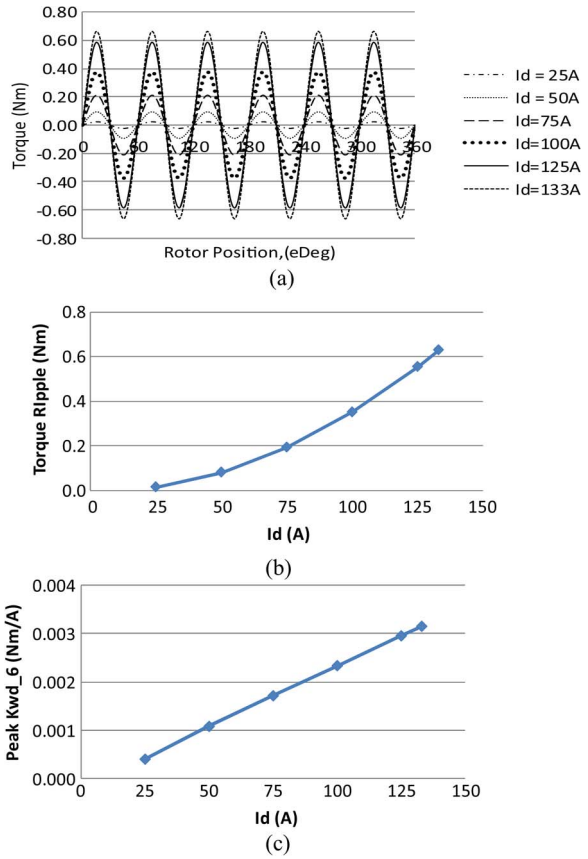

Fig. 6. (a) Developed electromagnetic torque by varying d-axis current and $I_q = 0$ A. (b) Sixth-order torque ripple magnitude. (c) Sixth-order motor constant magnitude.

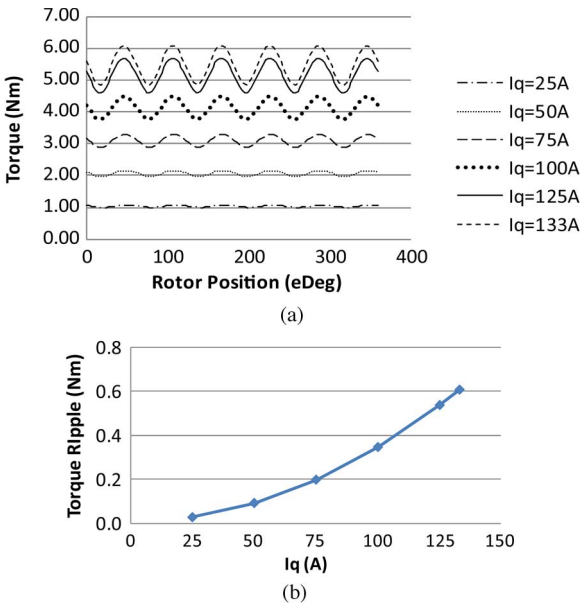

Fig. 7. (a) Electromagnetic torque. (b) Sixth-order torque ripple magnitude as a function if i_q.

the simulation at various phase current magnitudes and phases. The same set of simulation parameters as used in the previous section is repeated here. The results of the simulation are shown in Figs. 7 and 8.

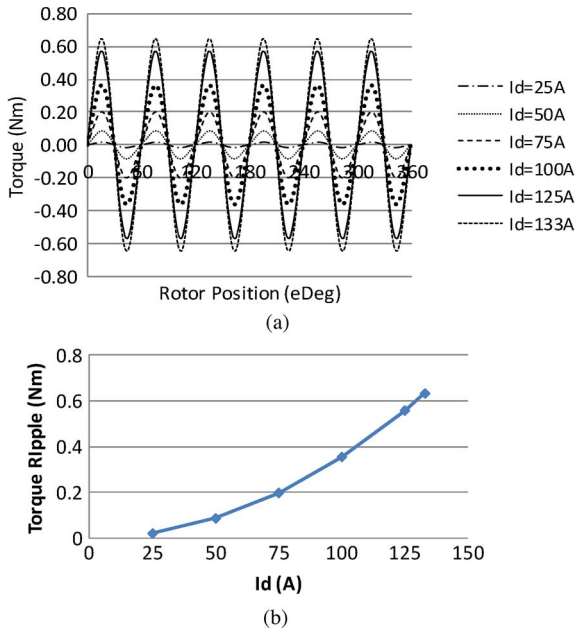

Fig. 8. (a) Electromagnetic torque. (b) Sixth-order torque ripple magnitude as a function of i_d.

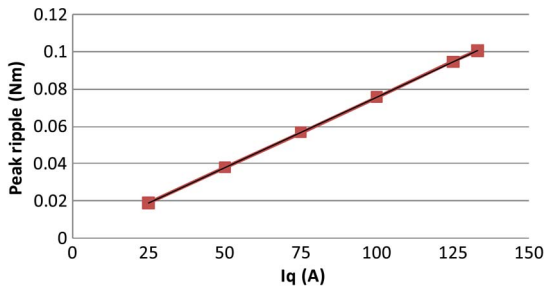

Fig. 9. Sixth harmonic peak torque ripple due to PM and i_q.

The effect introduced by the PM on the developed torque ripple can be deduced by vector subtraction of the results obtained from the torque simulation using with and without magnets. Fig. 9 shows the peak of the sixth-order torque ripple developed due to the interaction of the phase current and the PMs. A linearly increasing sixth-order peak torque ripple is observed as a function of the q-axis current, as shown in Fig. 9. This result shows that the motor constant K_{qm6} is a constant value, which is the same as found during the open-circuit simulation of back EMF constant ($K_{qm6} = 0.000505$ V $\cdot$ s/rad). The phase shift of the sixth-order torque ripple remains unchanged as a function of the q-axis current. The interaction of direct axis current and the PM have negligible effect for this particular design.

IV. Simulation and Experimental Results

A. Simulation Results of 9-Slot 6-Pole IPMSM

The proposed enhanced dynamic dq-model that includes the effect of torque ripple is implemented in MATLAB/Simulink. The PM is unmagnetized (Br $= 0$) in this model. The simulation is setup to run at constant peak current (75 A) with varying phase angles from 0° to 90° with respect to the q-axis. The

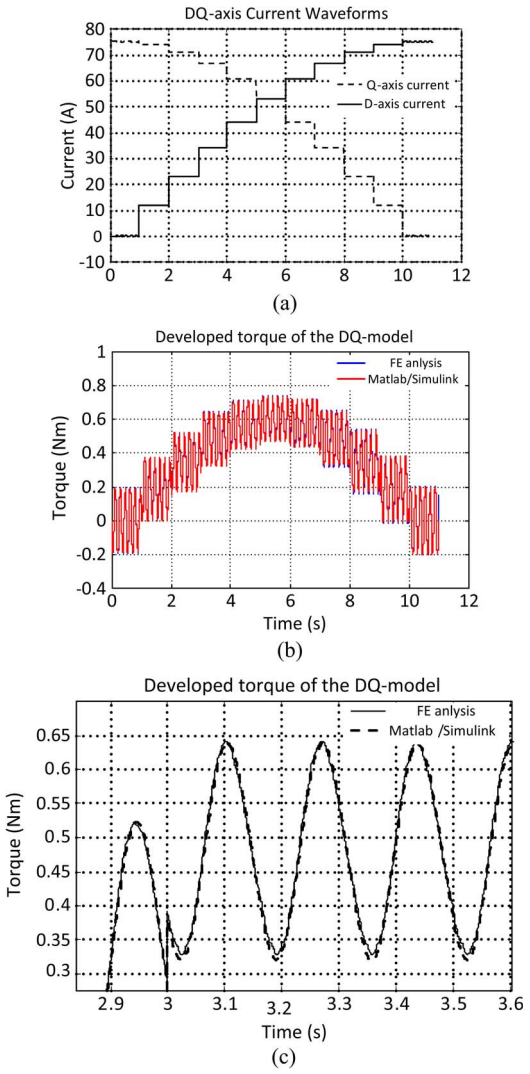

Fig. 10. (a) Applied q- and d-axes currents. (b) Simulation result of dq-model and FE analysis (torque developed). (c) Zoomed portion of Fig. 10(b).

same simulation parameters are used in the FE analysis. The result of the simulation is shown in Fig. 10. Fig. 10(b) shows the effect of the applied currents (q- and d-axis currents). Fig. 10(c) shows simulated torque of the dq-model and FE analysis at $I_q = 66.8$ A and $I_d = 34$ A. The simulation results of the proposed dq-model and the FE analysis shows good agreement for all combination of q- and d-axis current shown in Fig. 10(a).

B. Experimental Result of 9-Slot 6 Pole IPMSM

A 9-slot 6-pole three-phase IPMSM shown in Fig. 3 is built and tested. Some of the test conditions previously described during the model development has been tested to validate the modeling of the torque ripple. Torque ripple tests at different phase currents are performed. First, the motor was tested at 25, 50, 75, 100, 125, −25, −50, −75, −100, and −125 A, respectively with a phase angle of zero with respect to the q-axis. This particular setup forces i_q only while the d-axis current I_d is zero. Fig. 11 shows the effect of q-axis current on the developed peak torque ripple and phase. The torque ripple

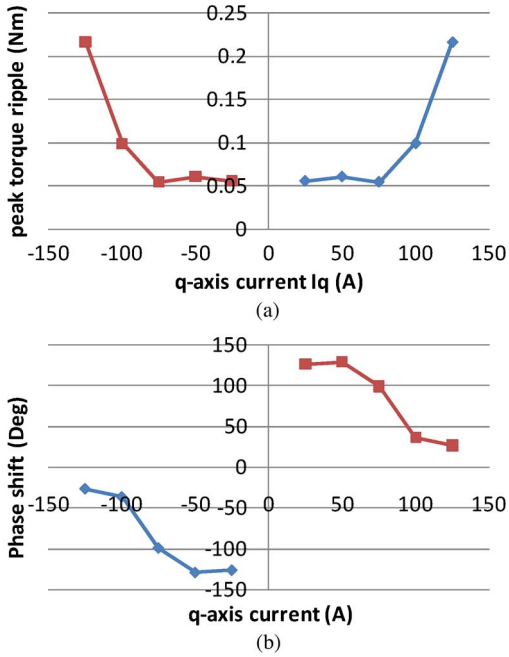

Fig. 11. (a) Sixth-order peak torque ripple due to I_q. (b) Phase of sixth-order torque ripple due to I_q.

magnitude depends on the magnitude of q-axis current only, as shown in Fig. 11(a). However, the torque ripple phase shift is a function of both magnitude and polarity of the q-axis current, as shown in Fig. 11(b). This effect can be explained using (25) and (26). The winding space distribution torque ripple component is independent of q-axis current polarity, as shown in (21). Hence, the phase of the reluctance ripple does not change with the polarity of the i_q current. On the other hand, the phase of the torque ripple component due to the PM shifts by 180° when the q-axis current polarity changes from positive to negative, as expressed in (9). This understanding is important for successful implementation of active torque ripple cancellation, whereas the drive undergoes four quadrant operations.

C. Test Procedure for Computing Equivalent Circuit Coefficients

The coefficients that depend on the airgap flux density (effect of the back EMF) can be obtained by performing an "open-circuit test" and measuring the voltage at the terminal of the motor and the speed of the motor, and use (19) to calculate the instantaneous value of the back EMF constant. This back EMF constant has all the harmonic contents needed for the equivalent circuit. This approach does not depend on the different slot–pole combination.

The components due to the interaction of the rotor saliency and winding space distribution are obtained by performing loaded condition test. A known I_q current keeping $I_d = 0$ or a known I_d current keeping $I_q = 0$ is applied and the torque ripple of the test is measured. The torque ripple contribution of the interaction between the rotor saliency and the winding space distribution is the vector subtraction of the measured torque ripple and the torque ripple due to the back EMF harmonics

TABLE I
TEST MOTOR SPECIFICATION

Parameter Name	Values	Unit
Number of Slots	9	-
Number of Poles	6	-
Stack Length	43	mm
Stator Outer Diameter	85	mm
K_{mq0}	0.02252	V/rad-s
L_q	0.00015	H
L_d	0.000096	H
R	0.009	Ω

and cogging torque of the test motor. This approach does not depend on the different slot–pole combination.

V. CONCLUSION

An enhanced dq-model for a PMSM capable of predicting average and ripple component of torque has been presented in this paper. A detailed analysis based on FE simulation has been presented. Simulation results obtained from FE analysis are used to calculate the model parameters. An actual motor is built to perform experimental tests to correlate the theoretical findings. The proposed model is unique in terms of predicting motor performances, including torque ripple. The understanding of torque ripple mechanism will further help to develop proper torque ripple mitigation schemes for such drives. The saturation effects were neglected in this study, which might affect the accuracy of the torque ripple depending on the design of the machine.

APPENDIX

See Table I.

REFERENCES

[1] G. Ombach and J. Junak, "Torque ripple optimization of skewed IPM motor for field weakening operation," in *Proc. ICEMS*, Aug. 20–23, 2011, pp. 1–7.
[2] M. Islam, S. Mir, T. Sebastian, and S. Underwood, "Design considerations of sinusoidally excited permanent magnet machines for low torque ripple applications," *IEEE Trans. Ind. Appl.*, vol. 41, no. 4, pp. 955–962, Jul./Aug. 2005.
[3] T. Sebastian, G. Slemon, and M. Rahman, "Modeling of permanent magnet synchronous motors," *IEEE Trans. Magn.*, vol. 22, no. 5, pp. 1069–1071, Sep. 1986.
[4] P. Pillay and R. Krishnan, "Modeling, simulation, analysis of permanent-magnet motor drives part I: The permanent-magnet synchronous motor drive," *IEEE Trans. Ind. Appl.*, vol. 25, no. 2, pp. 265–273, Mar./Apr. 1989.
[5] P. Pillay and R. Krishnan, "Modeling, simulation, analysis of permanent-magnet motor drives part II: The brushless motor drive," *IEEE Trans. Ind. Appl.*, vol. 25, no. 2, pp. 274–279, Mar./Apr. 1989.
[6] S. Rojas, M. A. Perez, J. Rodriguez, and H. Zelaya, "Torque ripple modeling of a permanent magnet synchronous motor," in *Proc. IEEE ICIT*, Mar. 14–17, 2010, pp. 433–438.
[7] T. Liu, I. Husain, and M. Elbuluk, "Torque ripple minimization with online parameter estimation using neural networks in permanent magnet synchronous motors," in *Conf. Rec. IEEE IAS Annu. Meeting*, Oct. 1998, vol. 1, pp. 35–40.
[8] J. F. Gieras, "Analytical approach to cogging torque calculation in PM brushless motors," in *Proc. IEEE IEMDC*, Jun. 1–4, 2003, vol. 2, pp. 815–819.
[9] D. Min, A. Keyhani, and T. Sebastian, "Torque ripple analysis of a PM brushless DC motor using finite element method," *IEEE Trans. Energy Convers.*, vol. 19, no. 1, pp. 40, 45, Mar. 2004.
[10] N. Bianchi, M. Degano, and E. Fornasiero, "Sensitivity analysis of torque ripple reduction of synchronous reluctance and interior PM motors," in *Proc. IEEE ECCE*, Sep. 15–19, 2013, pp. 1842–1849.
[11] Y. Sozer and D. A. Torrey, "Adaptive torque ripple control of permanent magnet brushless DC motors," in *Proc. 13th Annu. APEC Expo.*, Feb. 15–19, 1998, vol. 1, pp. 86–92.
[12] Z. Peng, G. Y. Sizov, and N. A. O. Demerdash, "Comparison of torque ripple minimization control techniques in surface-mounted permanent magnet synchronous machines," in *Proc. IEEE IEMDC*, May 15–18, 2011, pp. 188–193.

Abraham Gebregergis (S'12–M'08–SM'06) received the B.Sc. degree from the University of Asmara (UOA), Asmara, Eritrea, in 2001, the M.Sc. degree from the University of Stellenbosch, Stellenbosch, South Africa, in 2004, and the Ph.D. degree from Clarkson University, Potsdam, NY, USA, in 2007, all in electrical engineering.

From 2001 to 2002, he was with the Department of Electrical Engineering, UOA, as an Assistant Lecturer. From 2008 to 2013, he was with Delphi Steering and Nexteer Automotive, Saginaw, MI, USA, as a Senior Electrical Engineer at the Innovation Center. Currently, he is a Chief Scientist with Halla Mechatronics, Bay City, MI, USA, where he is responsible for motor control for automotive applications. He has published several journal and conference papers. His research interests include electric machines and adjustable-speed drives.

Mazharul Huq Chowdhury (M'12–SM'11) received the B.Sc. degree from Bangladesh University of Engineering and Technology (BUET), Dhaka, Bangladesh, in 2006 and the M.A.Sc degree from Concordia University, Montreal, QC, Canada, in 2010, both in electrical engineering.

From 2006 to 2008, he was with Siemens as an Electrical Engineer. In 2011, he joined Nexteer Automotive, Saginaw, MI USA. Currently, he is a Senior Electromagnetic Engineer with Halla Mechatronics Bay City, MI, USA, where he is responsible for designing motors and sensors for both automotive and nonautomotive applications. His research interests include electric machines and adjustable-speed drives.

Mohammad S. Islam (S'99–M'00–SM'04) received the B.Sc. and M.Sc. degrees from Bangladesh University of Engineering and Technology (BUET), Dhaka, Bangladesh, in 1994 and 1996, respectively, and the Ph.D. degree from the University of Akron, Akron, OH, USA, in 2001, all in electrical engineering.

From 1994 to 1996, he was with the Department of Electrical and Electronic Engineering, BUET, as a Lecturer. From 2001 to 2013, he was with Delphi Steering and Nexteer Automotive, Saginaw, MI, USA, as a Staff Research Engineer at the Innovation Center. Currently, he is a Chief Scientist with Halla Mechatronics, Bay City, MI, USA, where he is responsible for motors, sensors, and electromagnetic actuators for automotive applications. He has published several journal and conference papers and currently holds 20 U.S. patents with several more pending. His research interests include electric machines and adjustable-speed drives.

Dr. Islam is currently serving as the Vice Chair of the Transportation Systems Committee and the Chair of the Awards Department of the IEEE Industry Applications Society.

Tomy Sebastian (S'80–M'86–SM'94–F'03) received the B.Sc. (Eng.) degree from the Regional Engineering College, Calicut, India, in 1979, the M.S. degree from the Indian Institute of Technology Madras, Chennai, India, in 1982, and the MA.Sc. and Ph.D. degrees from the University of Toronto, Toronto, ON, Canada, in 1984 and 1986, respectively.

From 1979 to 1980, he was with the Research and Development Center of KELTRON, Trivandrum, India. From 1987 to 1992, he was with the Research and Applied Technology Division, Black and Decker Corporation, Towson, MD, USA. From 1992 to 2013, he was with Delphi Saginaw Steering Systems and Nexteer Automotive, Saginaw, MI, USA, where his last responsibility was as Chief Scientist at the Innovation Center. Currently, he is the Director of Motor Drive Systems with Halla Mechatronics, Bay City, MI, USA. His areas of interests are electrical machines and variable-speed drives. He has over 50 technical publications and holds 25 U.S. patents.

Dr. Sebastian is a corecipient of an IEEE Industry Application Society (IAS) Transactions First Prize Paper Award. He is a recipient of the IEEE Industry Applications Society Outstanding Achievement Award. He has held several positions in the Industrial Drives Committee and in the Industrial Power Conversion Systems Departments of the IAS and is currently the Vice President of the IAS. He was the General Chair for the first IEEE Energy Conversion Congress and Exposition held in San Jose, CA, USA, September 20–24, 2009, and Co-General Chair of the IEEE Power Electronics, Drives and Energy Systems (PEDES 2012) held in Bengaluru, India.